

# **Air Bearing Effects on Actuated Thermal Pole-Tip Protrusion for Hard Disk Drives**

**Jia-Yang Juang and David B. Bogy**

Computer Mechanics Laboratory  
Department of Mechanical Engineering  
University of California at Berkeley  
Berkeley, CA 94720

## **ABSTRACT**

Flying height (FH) control sliders with thermal actuation have been introduced recently in commercial products for compensating the static FH loss and reducing the risk of head-disk contacts. In the research reported here we investigated the effects of ABS designs on the thermal actuation. We created a 3-D finite element model of an entire slider with detailed read/write transducer structure, and then we conducted thermal-structural coupled-field analysis using velocity slip and temperature jump boundary conditions to formulate the heat transfer across the head-disk interface when a slider flies over a spinning disk. An iteration procedure was used to obtain the equilibrium solutions. Four ABS designs with distinct features were simulated. We defined five measures of merit, including protrusion rate, actuation efficiency, power consumption, pressure peak and temperature rise of the sensor, to evaluate the performance of thermal actuation. It is found that the effect of the pressure is more significant than that of the FH on the heat conduction from the slider to the disk. The efficiencies of three conventional designs decrease as the FHs are continuously reduced. A new ABS design, called “Scorpion III”, is presented and it demonstrates an overall enhancement, including virtually 100 percent efficiency with significantly less power

consumption. Transient thermal analysis showed that it requires about 1-2 ms for the temperature to reach the steady-state values, and there is a trade-off between increasing the actuation bandwidth and decreasing the power consumption.

## ***1. INTRODUCTION***

With the increase of areal density in hard disk drives the physical spacing (or flying height, FH) between the read/write element and the surface of the disk has been continuously decreased. A spacing of about 2.5 nm is said to be required for a density of 1 Tbit/in<sup>2</sup>. At such a low FH static losses of the FH due to manufacturing tolerance, ambient pressure changes and temperature variations can cause head-disk contact and result in data loss. Furthermore, slider disk contacts must be avoided during load/unload processes and operational shocks. The dynamic instability caused by FH modulations (FHMs) and nanoscale adhesion forces, such as electrostatic and intermolecular forces, should be minimized. Those challenges make a conventional air bearing surface (ABS) slider an unlikely choice for 1 Tbit/in<sup>2</sup>. One potential solution is a FH adjustment or controlled slider that is capable of adjusting its gap FH. Due to their quick response and low power consumption piezoelectric materials have been proposed as active elements for adjusting the FH [1]-[8]. However, the requirements of the piezoelectric materials and the necessary modification of the slider design pose challenges in integration of the fabrication process and increase the manufacturing cost.

The read/write elements of a magnetic head slider consist of thin layers of different materials including write poles, sensor, shields, undercoat, overcoat, coil, insulation layer and the substrate. Due to the mismatch of the coefficients of thermal expansion of the various materials the pole-tip of the write pole protrudes below the ABS plane when the ambient temperature varies and/or when an internal heat source is generated by Joule heating of the write current. These temperature-induced (T-PTP) and write-induced (W-PTP) pole-tip protrusions adversely reduce the FH by several nanometers and increase the risk of head-disk

contact. Several groups have numerically and/or experimentally investigated the effects of T-PTP and W-PTP [9]-[17].

Based on this concept Meyer *et al.* [18] deposited a resistance heating element (heater) near the read/write elements, and the gap FH was reduced by applying a current through the heater to deliberately induce the pole-tip protrusion. Similarly, Kurita *et al.* developed an active head slider with a nano-thermal actuator [19]. They used a finite element method to calculate the temperature distribution and thermal protrusion of their slider. They found that the additional air pressure increase caused by the protrusion lifted the slider upward and the amount of FH reduction was 30 % less than the protrusion. In their study the distribution of the heat transfer coefficient on the ABS was assumed to be constant. However, the effect of heat conducted from the slider to the disk through the ABS is a strong function of both FH and air pressure distributions, and, hence, these two factors have to be considered in the model. Juang *et al.* [20] studied the actuation performance of an ABS slider with consideration of the effect of FH and pressure distributions. They found that even though the protruded area was relatively small there was still considerable air bearing coupling with the resulting actuation efficiency (defined as the ratio of FH reduction to protrusion) of only 63 %, which suggested that ABS played a key role in the actuation performance. Therefore, it is highly desirable to have a better understanding of the effects of the ABS on the thermal actuation and to provide design guidelines for improving the performance.

In this report we study the effects of the ABS on thermal actuation by numerical simulation. A three-dimensional thermal-structural coupled field finite element model is created with detailed structures of read/write and heating elements. The cooling effect of the air bearing is included in the model as thermal boundary conditions. Steady-state and

transient analyses of four ABSs with distinct features are presented. We found that a properly designed ABS can significantly improve the actuation efficiency and power consumption of a FH control slider with thermal acuation.

## 2. *NUMERICAL MODELING AND ANALYSIS*

The temperature distribution and thermal deformation of a slider body with thermal actuation are determined by the configuration, dimensions and material properties of the read/write and heating elements and boundary conditions. The heat transfer boundary conditions depend on the flying state of the slider and hence the air bearing surfaces. In this study we kept the structure of the transducers the same and investigated the effect of ABS on actuation performance. We created a three-dimensional finite element model of an entire slider (length = 1.25 mm, width = 1.00 mm, thickness = 0.30 mm) with detailed read/write transducer structure as shown in Fig. 1. The slider has a single-layer 5-turn copper coil, a yoke width of 12  $\mu\text{m}$ , and a write track width of 1  $\mu\text{m}$ . The top and bottom poles are 1  $\mu\text{m}$  thick. The top and bottom magnetic shields are 2  $\mu\text{m}$  thick. The heating element has a thickness of 250 nm, and it is located between the coil and bottom pole. The photoresist layer, undercoat insulation layer and overcoat are also included in the model. The material properties and thickness of each layer are shown in Table I. These values, in particular the thermal conductivity, are process-dependent and we used the data published in various papers [10], [14], [21], [22]. A series of thermal-structural coupled-field finite element analyses have been carried out using ANSYS, a commercial finite element package, to study the actuation performance of the thermal nanoactuator. The air bearing modeling was done using the CML Air Bearing Simulator, which solved the generalized Reynolds equation to obtain the steady-state flying attitude.

At the head-disk interface heat is transferred from the slider to the disk through the air bearing cooling effect. The cooling effect of the air bearing plays a key role in this 3-D heat transfer problem. Chen *et al.* [23] found that the dominant factor of this effect was heat conduction. They applied the slip condition for the velocity and the jump condition for the temperature at the boundaries of the air bearing and obtained the heat transfer model as follows:

$$q(x, y) = -k \frac{T_s(x, y) - T_d}{h(x, y) + 2b\lambda(x, y)} + f(.) \quad (1)$$

where  $T_s$  and  $T_d$  are the temperatures of the slider and the disk, respectively;  $b = 2(2 - \sigma_T) \gamma / \sigma_T (\gamma + 1) Pr$ ;  $h$  is the FH (air bearing thickness) of the slider; the mean free path of the air under pressure  $p$  is  $\lambda = \lambda_0 p_0 / p$ , while the thermal conductivity  $k$  is a very weak function of pressure.

Note that  $T_s$ ,  $h$  and  $\lambda$  are functions of the coordinates,  $x$  and  $y$ . For air at  $T = 300$  K and atmospheric pressure, the thermal conductivity  $k = 0.0263$  W/m K, the mean free path  $\lambda_0 = 65$  nm, and the Prandtl number  $Pr = 0.7$ . The specific heat ratio  $\gamma$  is 1.4 and the thermal accommodation coefficient  $\sigma_T$  is 0.9. We assume that the disk surface is kept at the ambient temperature  $T_d = 25$  °C. Since the first term on the right hand side of (1) is about 1-2 orders of magnitude larger than the other terms  $f(.)$ , only this term is modeled in this study. Unlike the ABS, the dominant factor of heat transfer at the non-ABS surfaces of the slider is heat convection with a coefficient on the order of  $100$  W/m<sup>2</sup> K.

The numerical iteration approach developed in [20] is adopted in this report. We first used the CML Air Bearing Simulator to obtain the nominal FH, pitch, roll and air pressure distribution of an ABS slider. Then we used Eq. (1) to specify the thermal boundary

condition at the ABS and calculated the temperature distribution of the slider body. The obtained temperature distribution was then used as the body load to solve the slider deformation and actuated pole-tip protrusion due to the temperature gradient and the mismatch of coefficient of thermal expansions of various materials. Since the thermal protrusion causes deformation of the ABS and hence changes the flying attitudes and the thermal boundary conditions, several iterations are required to achieve an equilibrium solution.

### **3. *RESULTS AND DISCUSSIONS***

#### **3.1 Four Air Bearing Designs**

We study the actuation performances of four ABS designs that have distinct flying attitudes and pressure distributions as shown in Fig. 2. Their flying attitudes are summarized in Table II. The first design, depicted in Fig. 2(a), is a five-pad design labeled CML-5nm. It was designed using an optimization algorithm for a nearly uniform 5-nm FH across the disk. The second design labeled Slider A is a three-pad design obtained from a commercial drive as shown in Fig. 2(b). It has three surfaces, each specifically designed to achieve the overall desired FH performance characteristics. The third and more complicated design is shown in Fig. 2(c) and labeled Slider B. This ABS was designed for sliders with thermal actuation and has recently been implemented in commercial products. Figures 3(a)-(c) show the pressure profiles normalized by the ambient pressure generated under the CML-5nm, Slider A and Slider B, respectively. The sliders are mainly supported by the high pressure peaks generated by the central trailing pads, which are typically used in commercial products. The high peak pressure helps to maintain the stiffness of the air bearings. However when the thermal

actuation is used to adjust the FH, the high peak pressure at the center trailing pad also corresponds to more molecules per unit volume to transport energy and thus most of the power generated by the heating element is dissipated through the air bearing, which decreases the amount of thermal protrusion and increases the required heating power. Besides, the actuation efficiency (defined as the FH reduction to A-PTP ratio) is limited due to the strong counter effect of air bearing push-back.

In order to increase the actuation efficiency and to reduce the power consumption we designed an ABS, named Scorpion III, as shown in Fig. 2(d). The pressure distributions exhibit a distinct pattern compared to conventional designs as shown in Fig. 3(d). Instead of supporting by the center pressure peak the slider is primarily supported by the high pressures generated at the side rails. Scorpion III was found to exhibit an overall enhancement in performance, compared with several conventional ABS designs [24].

### **3.2 Steady-State Analysis**

Fig. 4 shows the steady-state heat transfer film coefficients on the air bearing surfaces of the four designs obtained after several numerical iterations at a heating power of 20 mW. Only part of the ABS that is close to the trailing edge is plotted. The distances of the write gap and GMR sensor from the trailing edge are 33 and 36.5  $\mu\text{m}$ , respectively. The disk linear speeds and skew angles are given in Table II. It is seen that the heat transfer coefficients are not constant and they are indeed strong functions of both the FH and air pressure distributions. The peak values are about 1.6, 1.2, 1.4, and 0.2  $\text{MW}/\text{m}^2\cdot\text{K}$  for CML-5nm, Slider A, Slider B, and Scorpion, respectively. The value of the Scorpion ABS is about 83 % to 86 % less than those of Slider A and Slider B even though the FHs of the three designs are

similar, which clearly indicates that the effect of the pressure is more significant than the FH effect.

Figs. 5 and 6 show the comparisons of the temperature rise and heat flux of the four designs at 20 mW, respectively. The maximum temperature rises are 2.78, 2.52, 3.21 and 7.8 K for CML-5nm, Slider A, Slider B and Scorpion, respectively. The Scorpion ABS has a higher temperature increase due to its relatively low heat flux, whereas the temperature distribution of Slider B exhibits a different pattern from the others.

Using the temperature distributions as body loads in the finite element models, we carried out the static structural analysis to calculate the slider deformation. A comparison of the protrusion profiles is shown in Fig. 7. The maximum A-PTPs on the ABSs are found to be 3.86, 3.56, 4.54 and 6.86 nm for CML-5nm, Slider A, Slider B and Scorpion, respectively. As expected, the Scorpion slider achieves 51% more protrusion than the second highest one at the same heating power of 20 mW. Fig. 8 shows the protrusion profiles along the center line across the read/write elements, which indicates that the peaks of protrusions are located at the read/write elements as a result of the higher local temperature and higher coefficients of thermal expansion of the metal layers.

Fig. 9 shows the FH reductions as a function of the *dc* heating power. The results indicate that the FH reduction is not proportional to the power. Instead, quadratic expressions have been found to best fit the curves for all the ABSs. This nonlinearity is related to the fact that the air bearing becomes stiffer when the FH is reduced and the heat transfer across the air bearing also becomes more effective because of the increased pressure and reduced FH.

In order to evaluate the performance of thermal actuation we defined five measures of merit as follows:

1. Actuation efficiency (%): The ratio of FH reduction to A-PTP.
2. Power consumption (mW): The power required for lowering one unit of the FH.
3. Peak pressure increase (atm): The increase of pressure peak caused by the thermal protrusion.
4. Protrusion rate (nm/mW): The amount of protrusion per unit power.
5. Temperature rise of the sensor (K): The temperature rise of the GMR sensors as a function of FH.

Fig. 10 shows a comparison of the A-PTP as a function of the heating power. Scorpion exhibits an increase of 80 %, 104 %, and 63 % in the protrusion rate over CML-5nm, Slider A, and Slider B, respectively. Fig. 11 shows the actuation efficiency as a function of the FH for the four ABSs. It is noted that the efficiencies of CML-5nm, Slider A and Slider B monotonically decrease as the FHs are reduced by the thermal protrusions and the values range from 40 % to 60 %. However, Scorpion demonstrates virtually 100 percent efficiency, which does not depend on the FH. The heating powers required for lowering the FHs are shown in Fig.12. The Scorpion ABS requires remarkably less power for reducing the FH from 10 nm to 3 nm compared to the other designs. Another important parameter that has to be considered is the pressure increase due to the deformed ABS. Fig. 13 shows that the peak pressures of Slider A and Slider B are 84 and 149 *atm*, respectively, when the FHs are reduced to about 3 nm. Such high pressures may not be physical in reality and may cause adverse effects. Since the Scorpion slider is supported by the two side pressure peaks and the pressure underneath the center pad is relatively low, the thermal protrusion of the center pad does not affect the pressure distribution.

The temperature rise of the read/write elements is of great concern in the thermal nanoactuator. The read-back signal of GMR sensors can be significantly altered by thermal influences since their electrical resistance is temperature dependent. Fig. 14 shows the temperature rises of the sensors as a function of the FH. It is observed that Scorpion has less temperature rise at FHs over 5 nm compared to Slider A and Slider B. The temperatures of Slider A and Slider B decrease when the FHs are reduced to less than 5 nm due to the highly concentrated pressures.

### **3.3 Transient Analysis**

The bandwidth of thermal actuation is of great importance because it determines the response time of the thermal protrusion to the heating power. A transient thermal study was conducted to investigate the bandwidth of the thermal protrusion when the slider flies over a disk. The power required for the first one nanometer FH reduction for each of the ABSs was applied from 0 to 2.5 ms and was turned off at 2.5 ms. The temperature changes of the GMR sensors were monitored as shown in Fig. 15. It requires about 1-2 ms for the read/write transducers to reach their steady-state values, corresponding to a bandwidth of 0.5-1 kHz. It is also seen that Scorpion has the least temperature rise and it takes longer to reach its steady-state value, which implies a trade-off between increasing the bandwidth and decreasing the temperature rise of the sensors.

## **4. CONCLUSIONS**

The effects of ABS on thermal actuation have been studied by numerical simulation. A series of three-dimensional thermal-structural finite element analyses were conducted using velocity slip and temperature jump boundary conditions to formulate the heat transfer

across the head-disk interface. An iteration procedure was used to obtain the equilibrium solutions. Four ABS designs with distinct features were simulated. In order to evaluate the performance of thermal actuation we defined five measures of merit, including protrusion rate, actuation efficiency, power consumption, pressure peak and temperature rise of the sensor. We found that the efficiencies of three conventional designs decrease as the FHs are continuously reduced. A new slider, Scorpion, which meets all design and fabrication requirements, has been presented and exhibits an overall enhancement, including virtually 100 % efficiency with significantly less power consumption. Quadratic expressions have been found to best fit the curves of the FH reduction as a function of the heating power for all the designs.

Transient thermal analysis of the sliders in the flying conditions with a varying heating power showed that about 1-2 ms are required for the temperature to reach the steady-state values. It is found that Scorpion has the least temperature rise of the GMR sensor at the first one nanometer FH reduction but the response time was longer than the other three designs. Therefore there is a trade-off between increasing the actuation bandwidth and decreasing the power consumption.

#### **ACKNOWLEDGEMENT**

This study is supported by the Computer Mechanics Laboratory (CML) at the University of California, Berkeley and the Information Storage Industry Consortium (INSIC). J. Y. Juang has also been supported by The California State Nanotechnology Fellowship. J. Y. Juang would like to thank Dr. Li Xu for helpful discussions on the heat transfer problem of micro- and nano scale devices.

## REFERENCES

1. C. E. Yeack-Scranton, V. D. Khanna, K. F. Etzold, and A. P. Praino, "An active slider for practical contact recording," *IEEE Trans. Magn.*, vol. 26, pp. 2478-2483, 1990.
2. M. Kurita and K. Suzuki, "Flying-height adjustment technologies of magnetic head sliders," *IEEE Trans. Magn.*, vol. 40, pp. 332-336, 2004.
3. K. Suzuki, R. Maeda, J. Chu, T. Kato, and M. Kurita, "An active head slider using a piezoelectric cantilever for in situ flying-height control," *IEEE Trans. Magn.*, vol. 39, pp. 826-831, 2003.
4. N. Tagawa, K.-I. Kitamura, and A. Mori, "Design and fabrication of MEMS-based active slider using double-layered composite PZT thin film in hard disk drives," *IEEE Trans. Magn.*, vol. 39, pp. 926-931, 2003.
5. L. Su, M. Kurita, J. Xu, K. Kato, K. Adachi, and Y. Miyake, "Static and dynamic characteristics of active-head sliders," *Tribol. Intl.*, vol. 38, pp. 717-723, 2005.
6. J. Y. Juang and D. B. Bogy, "Controlled-flying proximity sliders for head-media spacing variation suppression in ultralow flying air bearings," *IEEE Trans. Magn.*, vol. 41, pp. 3052-3054, 2005.
7. J. Y. Juang and D. B. Bogy, "Nonlinear compensator design for active sliders to suppress head-disk spacing modulation in hard disk drive," *IEEE/ASME Trans. Mechatron.*, to be published.
8. J. Y. Juang, D. B. Bogy and C. S. Bhatia, "Numerical and experimental studies of an Al<sub>2</sub>O<sub>3</sub>-TiC slider with a piezoelectric nanoactuator," *2006 ASME/JSME Joint Conf. on Micromechatronics for Information and Precision Equipment*, June 21-23, Santa Clara, CA.

9. B. K. Gupta, K. Young, S. K. Chilamakuri, and A. K. Menon, "On the thermal behavior of giant magnetoresistance heads," *ASME J. of Tribol.*, vol. 123, pp. 380-387, 2001.
10. L. Pust, C. J. T. Rea, and S. Gangopadhyay, "Thermo-mechanical head performance," *IEEE Trans. Magn.*, vol. 38, pp. 101-106, 2002.
11. W. Yan, "Thermal pole tip protrusion finite element analysis of thin film inductive recording heads," *J. of Applied Physics*, vol. 91, pp. 7571-7573, 2002.
12. R. H. Wang, X. Z. Wu, W. Weresin, and Y. S. Ju, "Head protrusion and its implications on head-disk interface reliability," *IEEE Trans. Magn.*, vol. 37, pp. 1842-1844, 2001.
13. J. Xu, M. Kurita, and M. Tokuyama, "Thermal analysis of a magnetic head," *IEEE Trans. Magn.*, vol. 40, pp. 3142-3144, 2004.
14. Y. S. Ju, "Self-heating in thin-film magnetic recording heads due to write currents," *IEEE Trans. Magn.*, vol. 41, pp. 4443-4448, 2005.
15. K. Aoki, T. Hoshino, T. Iwase, T. Imamura, and K. Aruga, "Thermal pole-tip protrusion analysis of magnetic heads for hard disk drives," *IEEE Trans. Magn.*, vol. 41, pp. 3043-3045, 2005.
16. V. Nikitin, S. Gider, J. Tabib, D. Hsiao, M. Salo, G. Sui, S. Yuan, N. A. Satoh, J. Xu, and Y. Maruyama, "Spatial and temporal profiling of protrusion in magnetic recording heads," *IEEE Trans. Magn.*, vol. 40, pp. 326-331, 2004.
17. E. Jang, G. Wang, K. Y. Cho, and H. Lee, "Heating and cooling effect of giant magnetoresistive heads during writing operations," *J. Applied Physics*, vol. 91, pp. 8769-8771, 2002.
18. D. W. Meyer, P. E. Kupinski, and J. C. Liu, "Slider with temperature responsive transducer positioning," U. S. Patent 5,991,113, Nov. 23, 1999.

19. M. Kurita, T. Shiramatsu, K. Miyake, A. Kato, M. Soga, H. Tanaka, S. Saegusa and M. Suk, "Active flying-height control slider using MEMS thermal actuator," *Microsyst. Technol.*, vol. 12, pp. 369-375, 2006.
20. J. Y. Juang, D. Chen, and D. B. Bogy, "Alternate air bearing slider designs for areal density of 1 Tbit/in<sup>2</sup>," *IEEE Trans. Magn.*, vol. 42, pp. 241-246, 2006.
21. Y. Yang, S. Shojaeizadeh, J. A. Bain, J. G. Zhu and M. Asheghi, "Detailed modeling of temperature rise in giant magnetoresistive sensor during an electrostatic discharge event," *J. Applied Physics*, vol. 95, pp. 6780-6782, 2004.
22. S. M. Lee and D. G. Cahill, "Thermal conductivity of sputtered oxide films," *Physical Review B*, vol. 52, pp. 253-257, 1995.
23. L. Chen, D. B. Bogy, and B. Strom, "Thermal dependence of MR signal on slider flying state," *IEEE Trans. Magn.*, vol. 36, no. 5, pp. 2486-2489, Sep. 2000.
24. J. Y. Juang and D. B. Bogy, "Design and analysis of a flying height control slider with thermal nanoactuator," Technical Report No. 2006-004, Computer Mechanics Lab., Department of Mechanical Engineering, University of California, Berkeley.

TABLE I  
Material Properties used in the FEA [13]-[16]

Layer and Material		Young's modulus (GPa)	Thermal conductivity (W/m.K)	Coefficient of thermal expansion ( $\times 10^{-6}/^{\circ}\text{C}$ )	Specific heat (J/kg.K)	Poisson's ratio
Slider substrate	Al <sub>2</sub> O <sub>3</sub> -TiC	380	20	7.9	878	0.3
Under-coat (1.2 $\mu\text{m}$ )	Al <sub>2</sub> O <sub>3</sub>	200	1.5	7.5	760	0.25
Shields (2.0 $\mu\text{m}$ )	Ni-Fe	207	35	12.2	470	0.3
Bottom pole (1.0 $\mu\text{m}$ )	Ni-Fe	207	35	12.2	470	0.3
Coil (2 $\mu\text{m}$ )	Cu	120	395	16.5	390	0.33
Heater (250 nm)	Ni-Fe (thin layer)	207	30	12.2	470	0.3
Coil insulation (5 $\mu\text{m}$ )	Photo-resist	7	0.19	51.0	1460	0.2
Top pole (1.0 $\mu\text{m}$ )	Ni-Fe	207	35	12.2	470	0.3
Overcoat (39.7 $\mu\text{m}$ )	Al <sub>2</sub> O <sub>3</sub>	200	1.5	7.5	760	0.25

TABLE II  
COMPARISON OF FLYING ATTITUDES AT THE MD

	FH (nm)	Pitch ( $\mu$ rad)	Roll ( $\mu$ rad)	Peak pressure (atm)	Linear velocity (m/s)	skew ( $^{\circ}$ )
CML-5nm	5.3	220	0.9	18.9	17.3	9.10
Slider A	11.5	130	-1.2	23.4	37.5	-2.56
Slider B	12.0	115	2.4	21.0	18.0	-2.56
Scorpion III	10.5	124	-0.4	38.0	37.5	-2.56

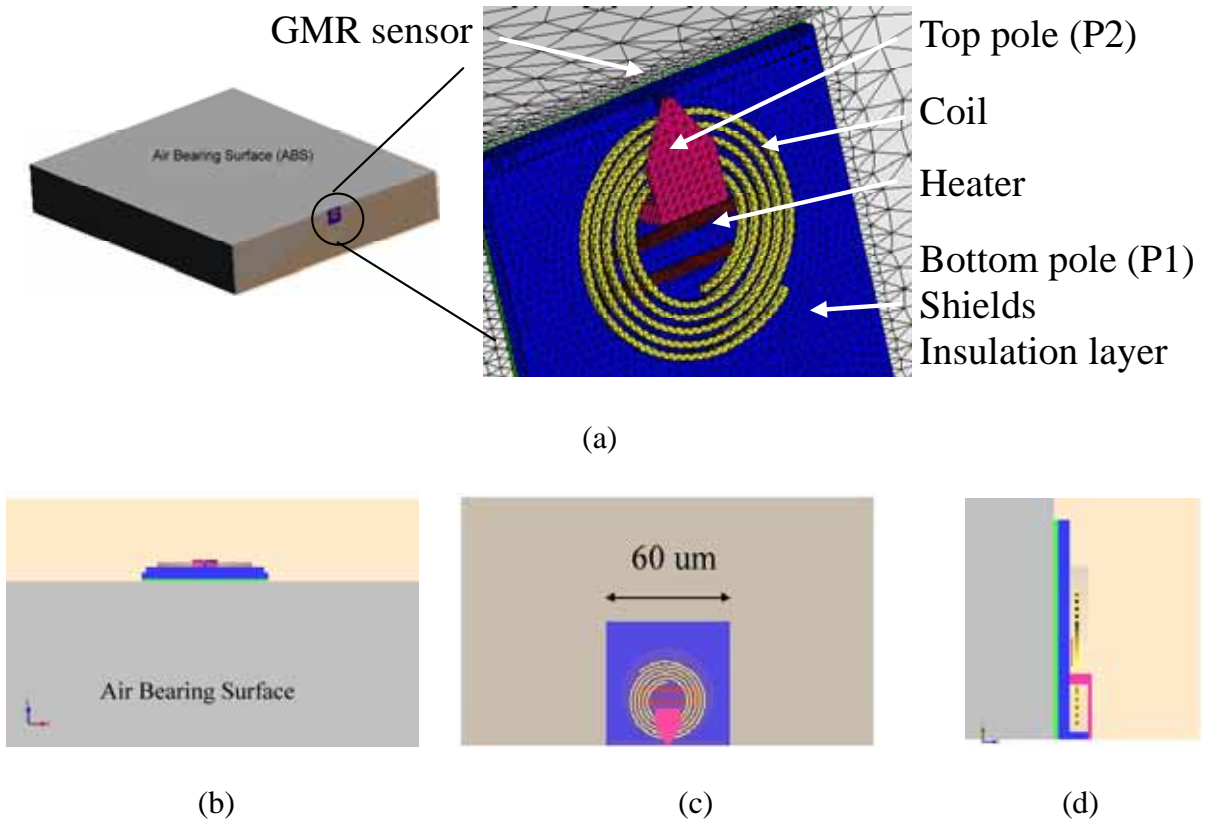
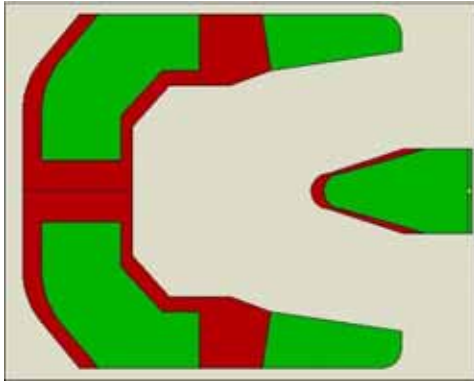
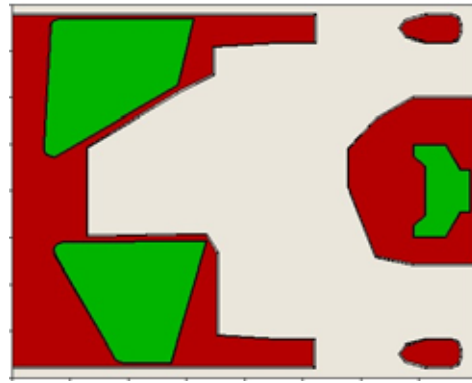


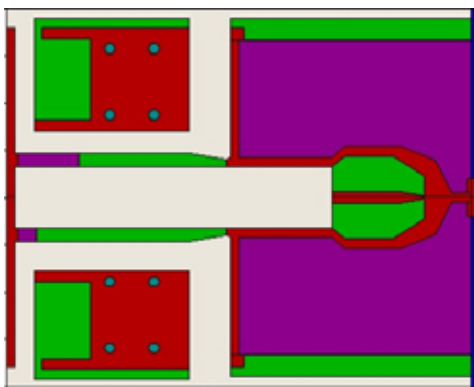
Fig. 1. The finite-element model of a FH control slider with thermal actuation. The overcoat and photoresist are not shown for a clear view of the read/write transducer. The protective carbon overcoat on the ABS and the pole-tip recession are not considered.



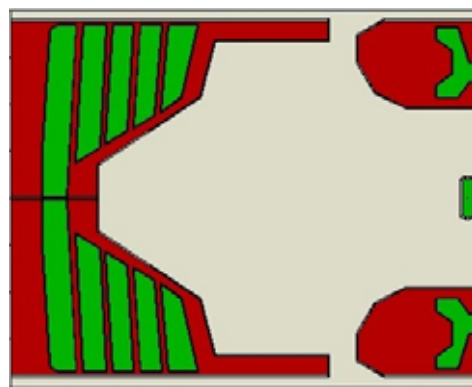
(a) CML-5nm



(b) Slider A

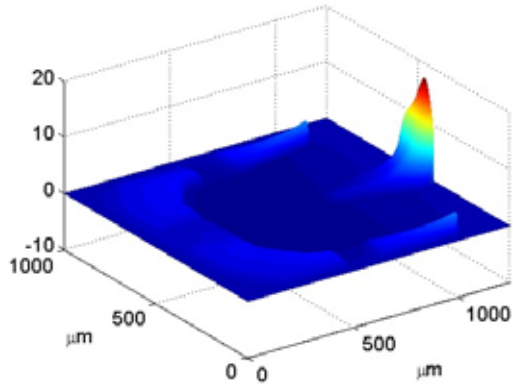


(c) Slider B

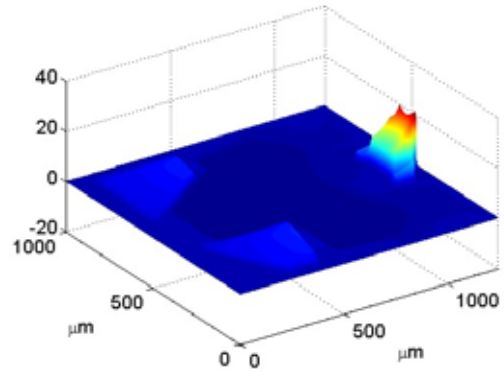


(c) Scorpion III

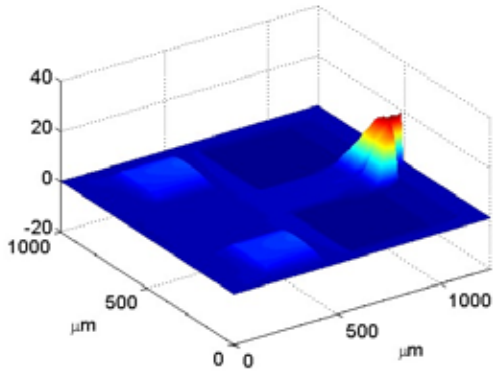
Fig. 2. Four ABS designs used in this study (length: 1.25 mm; width: 1.00 mm). Different colors indicate different etching levels.



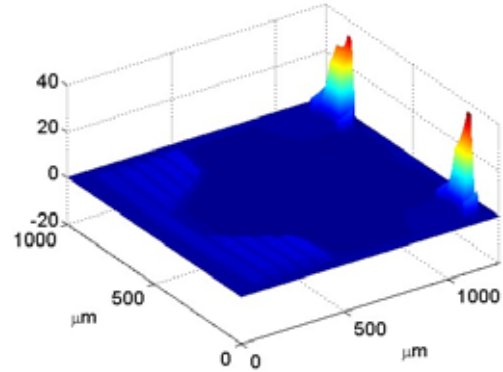
(a) CML-5nm (peak: 18.9 atm)



(b) Slider A (peak: 23.4 atm)

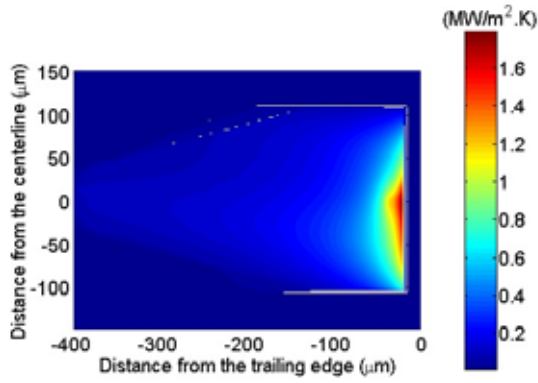


(c) Slider B (peak: 21.0 atm)

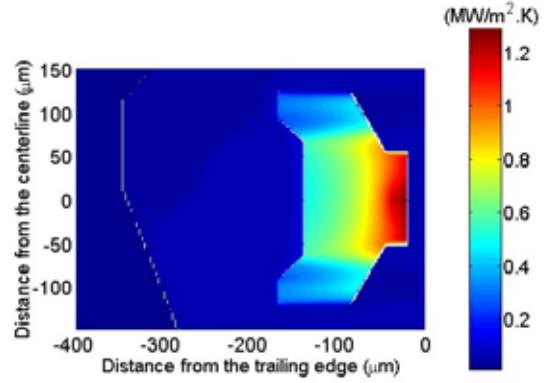


(d) Scorpion III (peak: 38.0 atm)

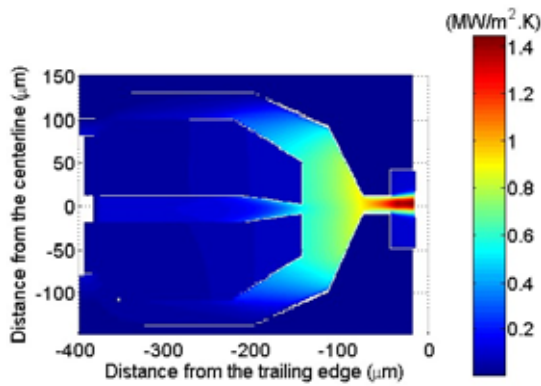
Fig. 3. The air pressure distributions of the ABS sliders. The scale displayed is normalized to ambient pressure:  $(p - p_a)/p_a$ .



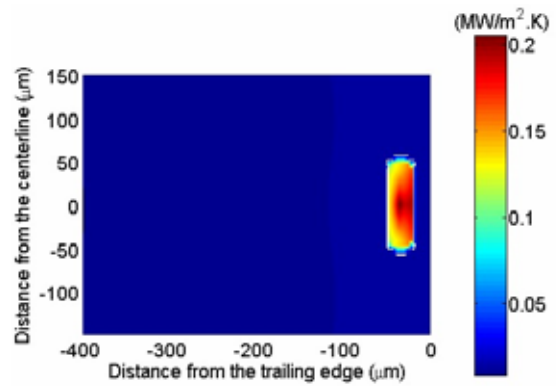
(a) CML-5nm



(b) Slider A

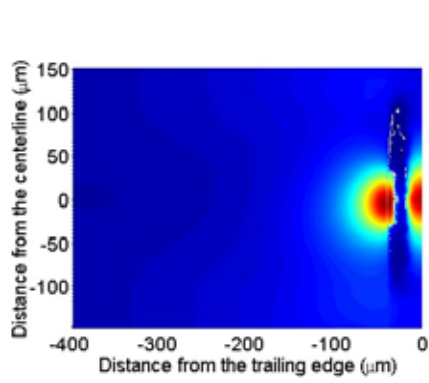


(c) Slider B

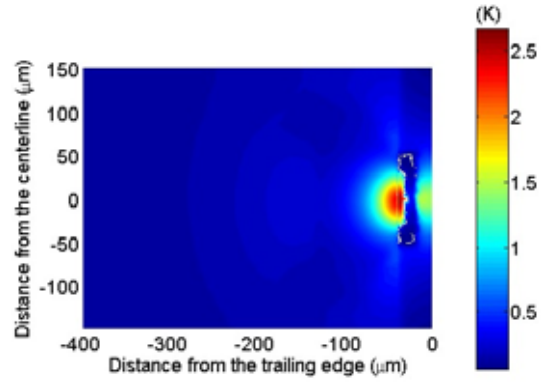


(d) Scorpion III

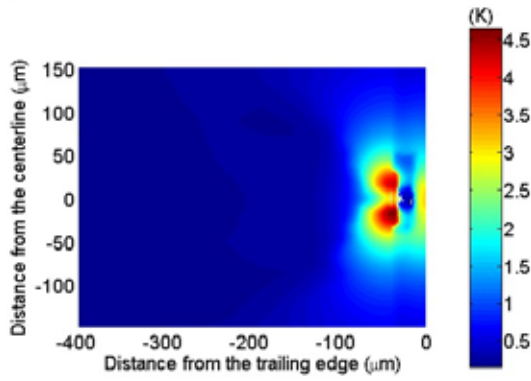
Fig. 4. The distributions of the heat transfer film coefficients on the air bearing surfaces at a heating power of 20 mW. Only part of the ABS that is close to the trailing edge is plotted. The distances of the write gap and the GMR sensor from the trailing edge are 33 and 36.5  $\mu\text{m}$ , respectively.



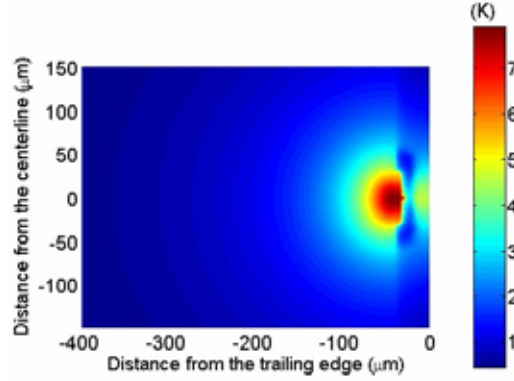
(a) CML-5nm



(b) Slider A

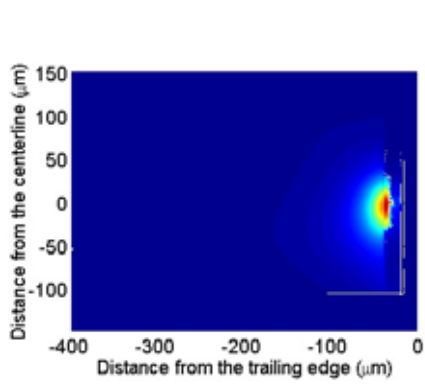


(c) Slider B

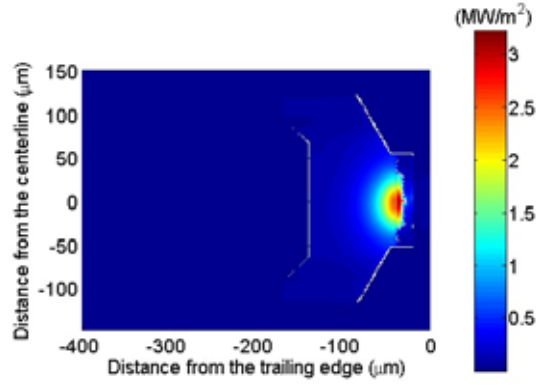


(d) Scorpion III

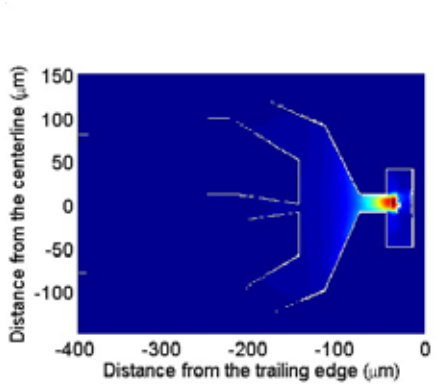
Fig. 5. The distributions of the temperature rises on the ABSs at a heating power of 20 mW.



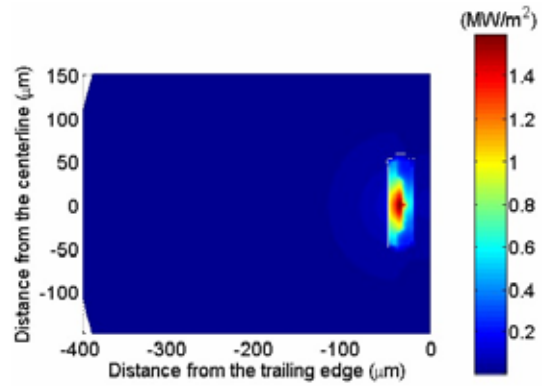
(a) CML-5nm



(b) Slider A

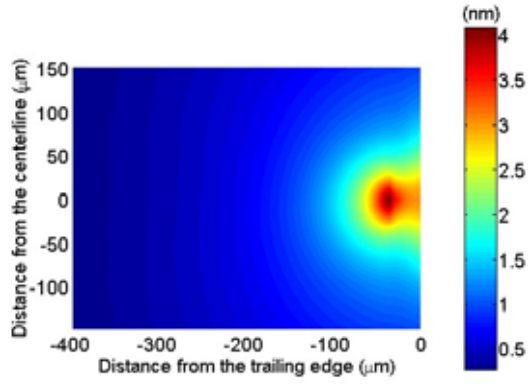


(c) Slider B

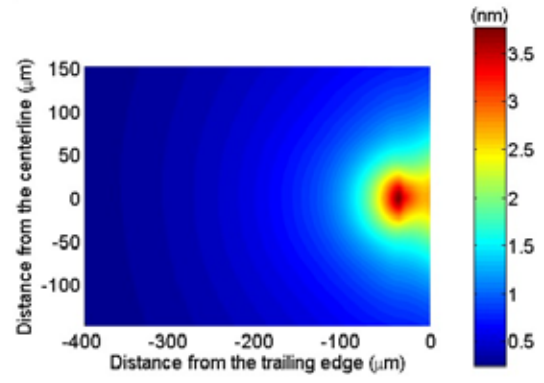


(d) Scorpion III

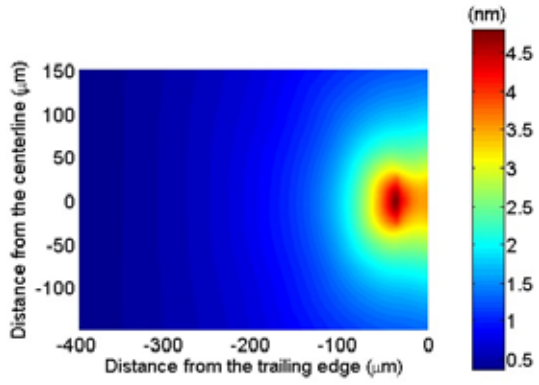
Fig. 6. The distributions of the heat flux on the ABSs at a heating power of 20 mW.



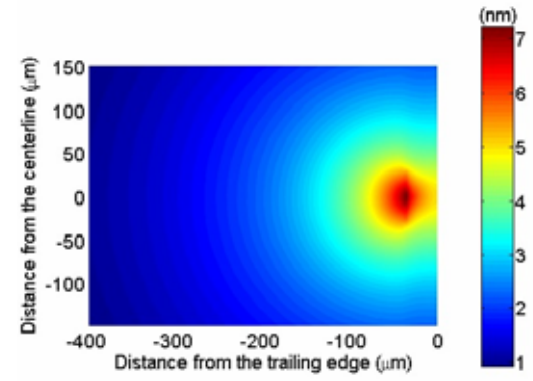
(a) CML-5nm



(b) Slider A



(c) Slider B



(d) Scorpion III

Fig. 7. The distributions of the A-PTP on the ABSs at a heating power of 20 mW.

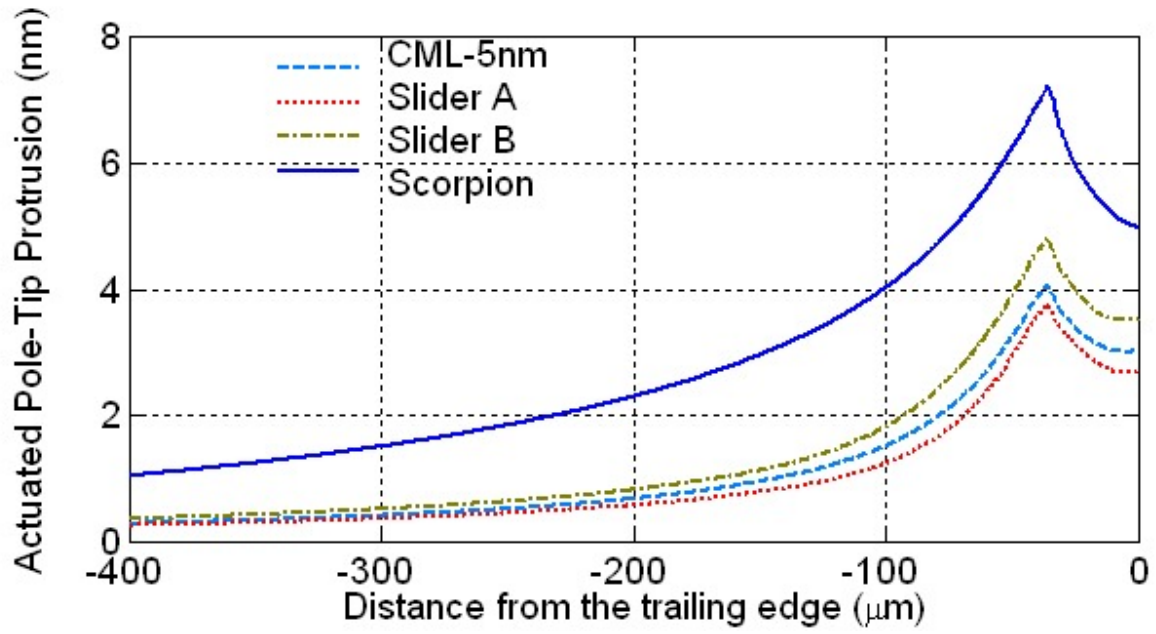
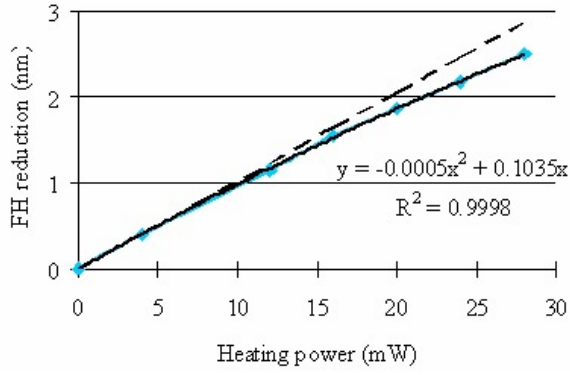
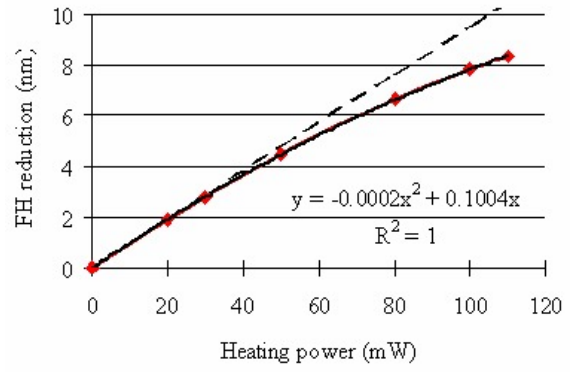


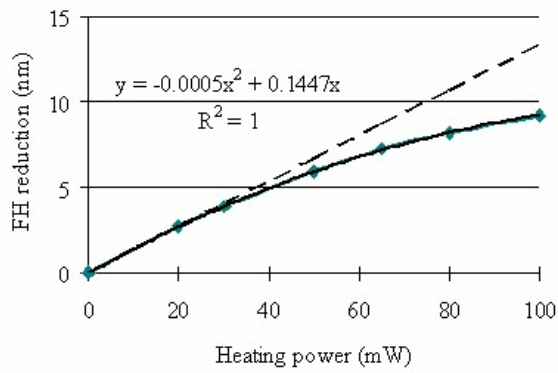
Fig. 8. Comparison of actuated thermal protrusion profiles of the four air bearings along the center line across the read/write element at a heating power of 20 mW.



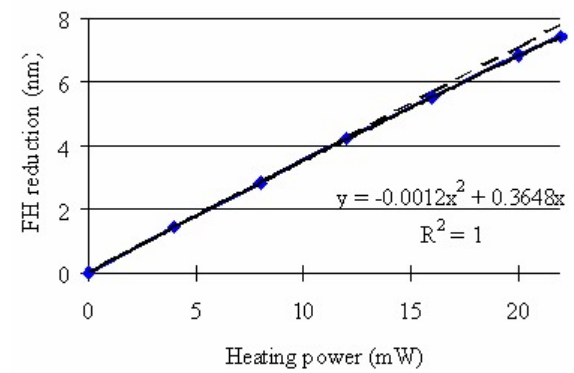
(a) CML-5nm



(b) Slider A



(c) Slider B



(d) Scorpion III

Fig. 9. The FH reductions as a function of heating power. The dash lines are the linear projections and the solid lines are quadratic fits to the data.

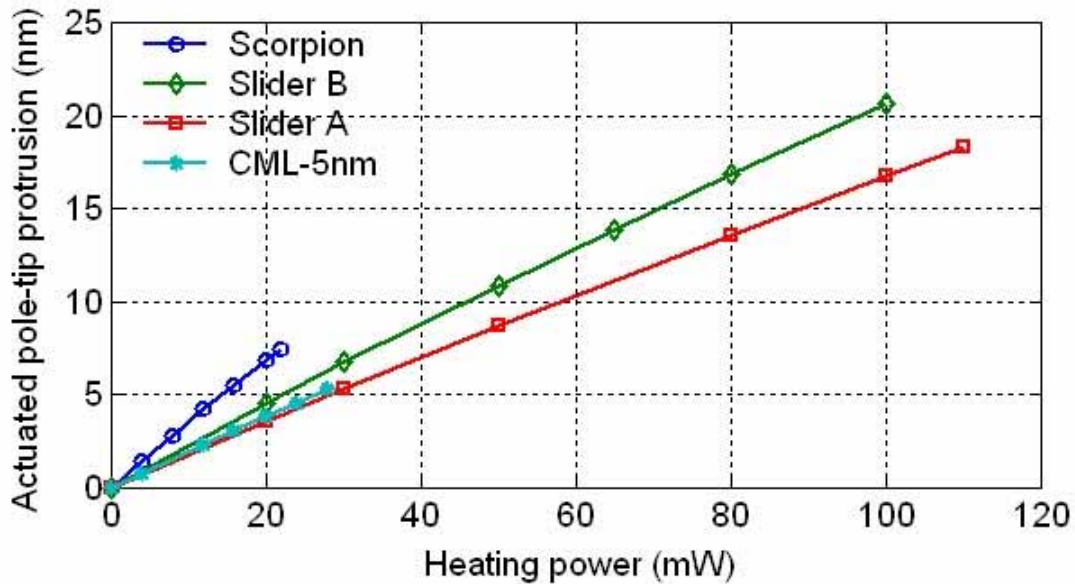


Fig. 10. A comparison of the A-PTP as a function of the heating power. The protrusion rates are about 0.19, 0.17, 0.21, and 0.34 nm/mW for CML-5nm, Slider A, Slider B, and Scorpion, respectively.

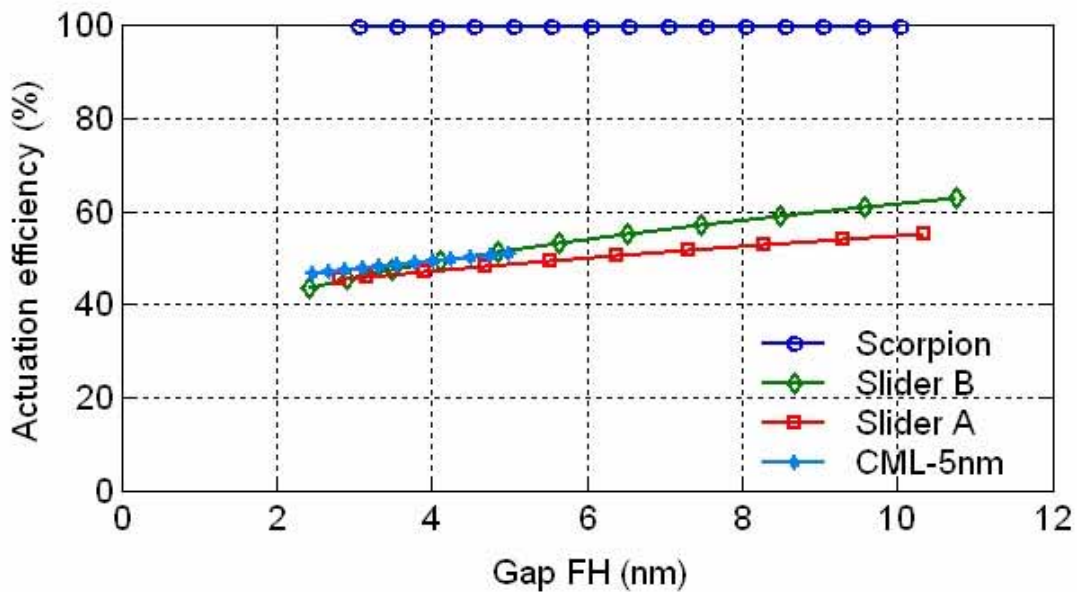


Fig. 11. A comparison of the efficiency as a function of the FH. The efficiencies of CML-5nm, Slider A and Slider B monotonically decrease as the FHs are reduced by the thermal protrusions and Scorpion demonstrates virtually 100 % efficiency.

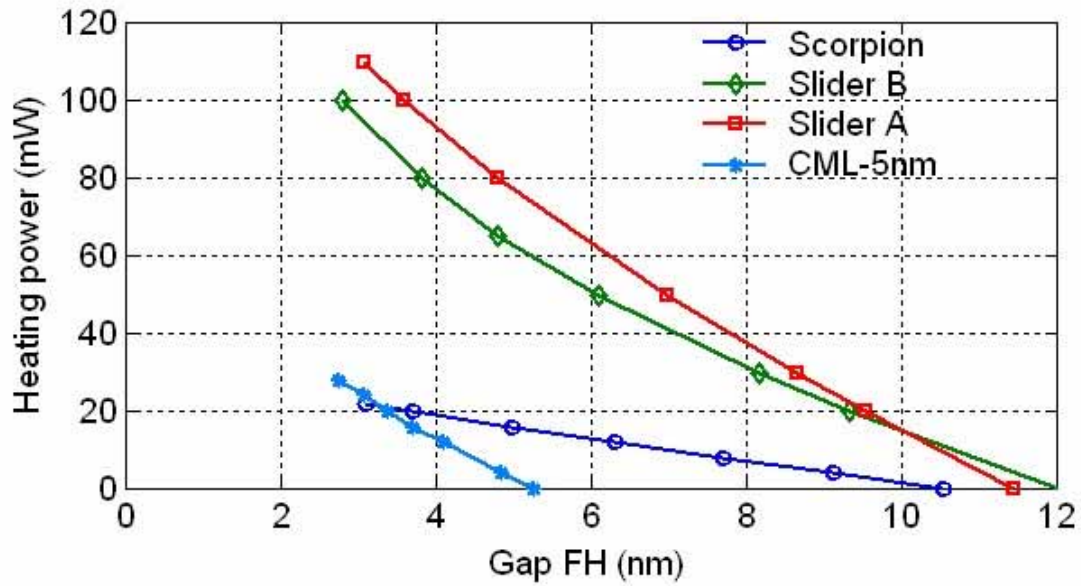


Fig. 12. The required heating power for reducing the FH.

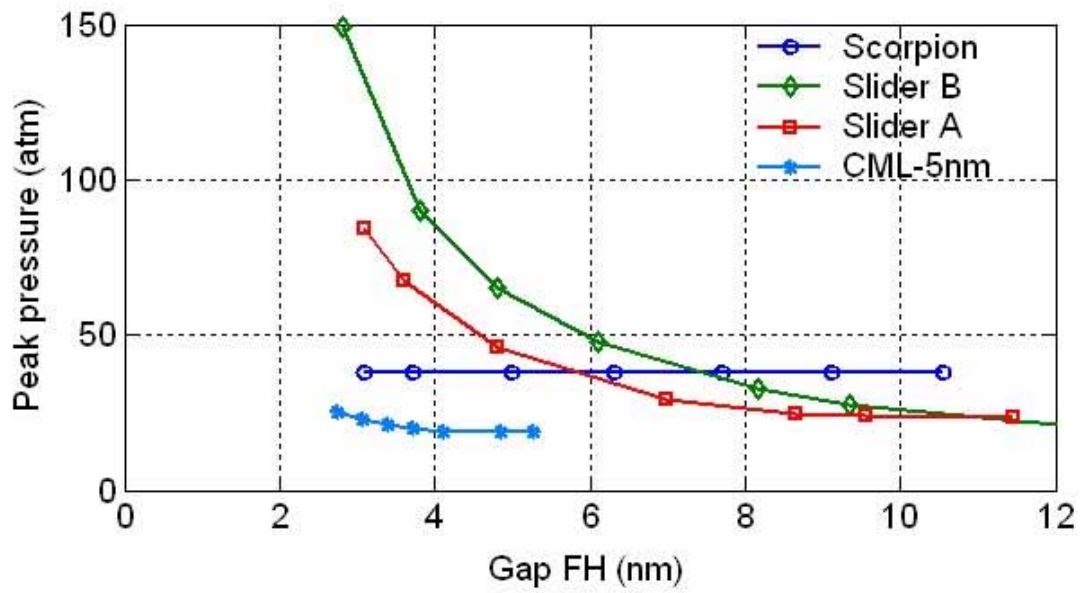


Fig. 13. A comparison of the peak pressures as functions of the FHs.

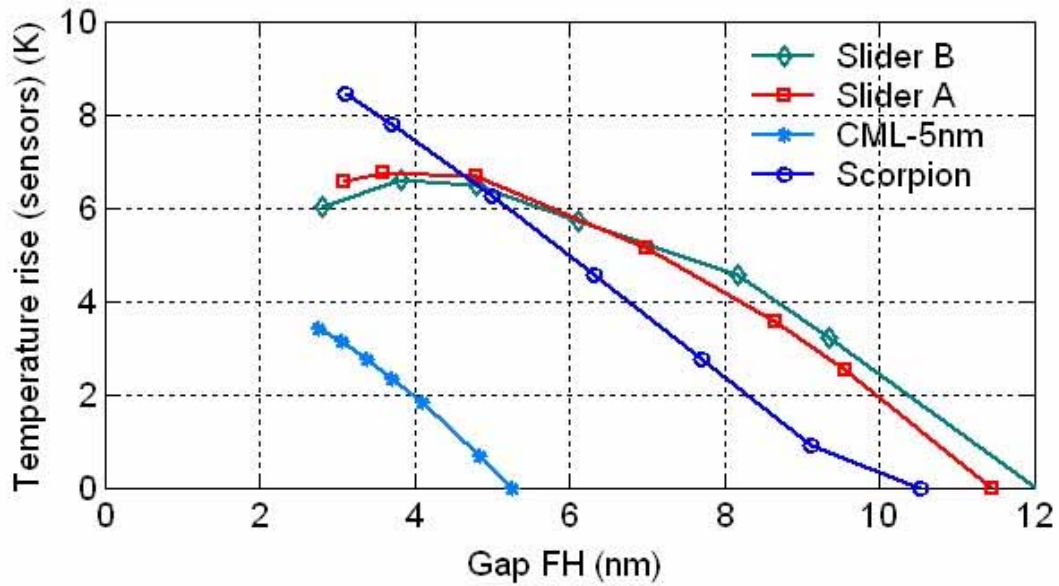
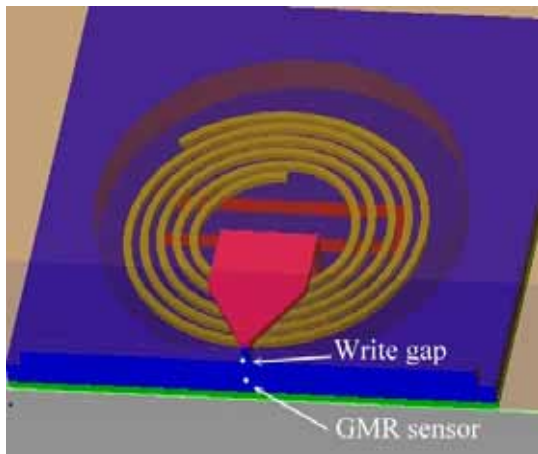
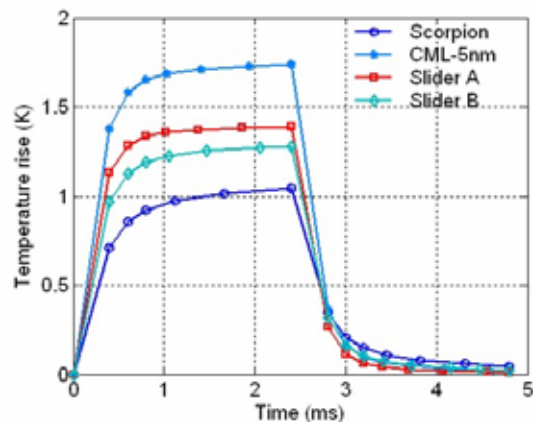


Fig. 14. The temperature rises of the sensors when the FHs are reduced by applying a heating power.



(a)



(b)

Fig. 15. Transient temperature changes of the flying sliders with a varying heating power. The power required for the first one nanometer FH reduction for each of the ABSs was applied from 0 to 2.5 ms and was turned off at 2.5 ms.